

https://doi.org/10.1130/G49879.1

Manuscript received 7 April 2021 Revised manuscript received 17 November 2021 Manuscript accepted 3 February 2022

Published online 11 April 2022

© 2022 Geological Society of America. For permission to copy, contact editing@geosociety.org

# Metastable olivine within oceanic lithosphere in the uppermost lower mantle beneath the eastern United States

Fansheng Kong<sup>1,2,3\*</sup>, Stephen S. Gao<sup>2</sup>, Kelly H. Liu<sup>2</sup>, Yinxia Fang<sup>1</sup>, Hejun Zhu<sup>4</sup>, Robert J. Stern<sup>4</sup> and Jiabiao Li<sup>1</sup>

¹Key Laboratory of Submarine Geosciences, Second Institute of Oceanography, Ministry of Natural Resources, Hangzhou 310012, China

²Geology and Geophysics Program, Missouri University of Science and Technology, Rolla, Missouri 65409, USA

³Southern Marine Science and Engineering Guangdong Laboratory, Zhuhai 519080, China

⁴Department of Geosciences, University of Texas at Dallas, Richardson, Texas 75080, USA

#### **ABSTRACT**

Approximately two-thirds of Earth's outermost shell is composed of oceanic plates that form at spreading ridges and recycle back to Earth's interior in subduction zones. A series of physical and chemical changes occur in the subducting lithospheric slab as the temperature and pressure increase with depth. In particular, olivine, the most abundant mineral in the upper mantle, progressively transforms to its high-pressure polymorphs near the mantle transition zone, which is bounded by the 410 km and 660 km discontinuities. However, whether olivine still exists in the core of slabs once they penetrate the 660 km discontinuity remains debated. Based on SKS and SKKS shear-wave differential splitting times, we report new evidence that reveals the presence of metastable olivine in the uppermost lower mantle within the ancient Farallon plate beneath the eastern United States. We estimate that the low-density olivine layer in the subducted Farallon slab may compensate the high density of the rest of the slab associated with the low temperature, leading to neutral buoyancy and preventing further sinking of the slab into the deeper part of the lower mantle.

### INTRODUCTION

Under thermodynamic equilibrium, olivine transforms to its high-pressure phases, wadsleyite at the 410 km seismic discontinuity (d410; Ringwood, 1975), which is the boundary between the upper mantle and the mantle transition zone (MTZ). Phase transition from wadsleyite to ringwoodite occurs at ~520 km, and from ringwoodite to bridgmanite and magnesiowüstite at the 660 km discontinuity (d660; Ito and Katsura, 1989), which separates the MTZ and the lower mantle. Olivine in subducting oceanic lithosphere (slabs) is also expected to undergo such phase transitions as it descends into the MTZ and the lower mantle. Due to the coolness of descending slabs relative to ambient mantle, metastable olivine inside the subducting plate can persist to >410 km deep (Iidaka and Suetsugu, 1992; Kirby et al., 1996; Jiang et al., 2008). Metastable olivine has lower density and seismic velocity in comparison to the high-density phases of the ambient mantle, and thus its existence in a descending slab can affect the subduction rate and the dipping angle of

mostly due to the expected small thickness of the metastable olivine layer in the lower mantle as compared to the resolution of seismic tomography images (Jiang et al., 2008; Kaneshima et al., 2007). In this study, we used results from the USArray seismic-station network (http://www.usarray.org/) to detect and characterize lowermantle seismic anisotropy based on shear-wave splitting analysis (Silver and Chan, 1991) and to demonstrate the existence of metastable olivine in the uppermost lower mantle beneath the eastern United States.

Shear-wave splitting analysis using shear waves refracted at the core-mantle boundary

the slab (e.g., Iidaka and Suetsugu, 1992; Kirby

et al., 1996; Bina and Kawakatsu, 2010; Agrusta

et al., 2014). However, whether metastable ol-

ivine can persist in the lower mantle is unclear,

Shear-wave splitting analysis using shear waves refracted at the core-mantle boundary (including SKS and SKKS; Fig. 1A) is widely utilized to detect and characterize anisotropy related to mantle flow and deformation (Silver and Chan, 1991; K.H. Liu et al., 2008; Grund and Ritter, 2019). When an SKS or SKKS wave travels through an azimuthally anisotropic layer with a horizontal axis of symmetry, it splits into two shear waves with orthogonal polarization

orientations and different propagation velocities (Silver and Chan, 1991). The different velocities result in a splitting delay time ( $\delta t$ ) between the fast and slow waves, which is closely related to the thickness of the anisotropic layer and magnitude of seismic anisotropy. The polarization orientation of the fast shear wave (also referred to as fast orientation or  $\varphi$ ) constrains the orientation of azimuthal anisotropy (Silver and Chan, 1991). While SKS and SKKS phases from the same earthquake recorded at the same station have nearly identical raypaths in the upper 500 km of the mantle, their raypaths in the lower mantle are significantly different (Grund and Ritter, 2019), with the former having a steeper angle of incidence (Fig. 1A). Therefore, the discrepancy between SKS and SKKS splitting measurements from the same event-station pair has been routinely utilized to explore lower-mantle anisotropy (Long and Lynner, 2015; Deng et al., 2017; Grund and Ritter, 2019). Such studies, however, mostly attribute the discrepant SKS-SKKS measurements to anisotropy in the lowermost layer of the lower mantle, while results from this study suggest that the major source of the discrepant measurements is located in the uppermost portion of the lower mantle.

We used shear-wave splitting discrepancies between SKS and SKKS phases measured from the same event-station pair to investigate the presence of metastable olivine in the uppermost lower mantle, which allowed us to further constrain the physical states of subducted Farallon lithosphere, slab buoyancy, and slab stagnation mechanism. Oceanic lithosphere of the Farallon plate subducted beneath the North American plate at ~80 mm/yr in a northeast direction from the Late Jurassic, ca. 165 Ma, to the mid-Cenozoic (L. Liu et al., 2008), ca. 25 Ma. Previous seismic tomography studies suggest that the subducted Farallon slab has two main

CITATION: Kong, F., et al., 2022, Metastable olivine within oceanic lithosphere in the uppermost lower mantle beneath the eastern United States: Geology, v. 50, p. 776–780, https://doi.org/10.1130/G49879.1

<sup>\*</sup>E-mail: kongfs@sio.org.cn

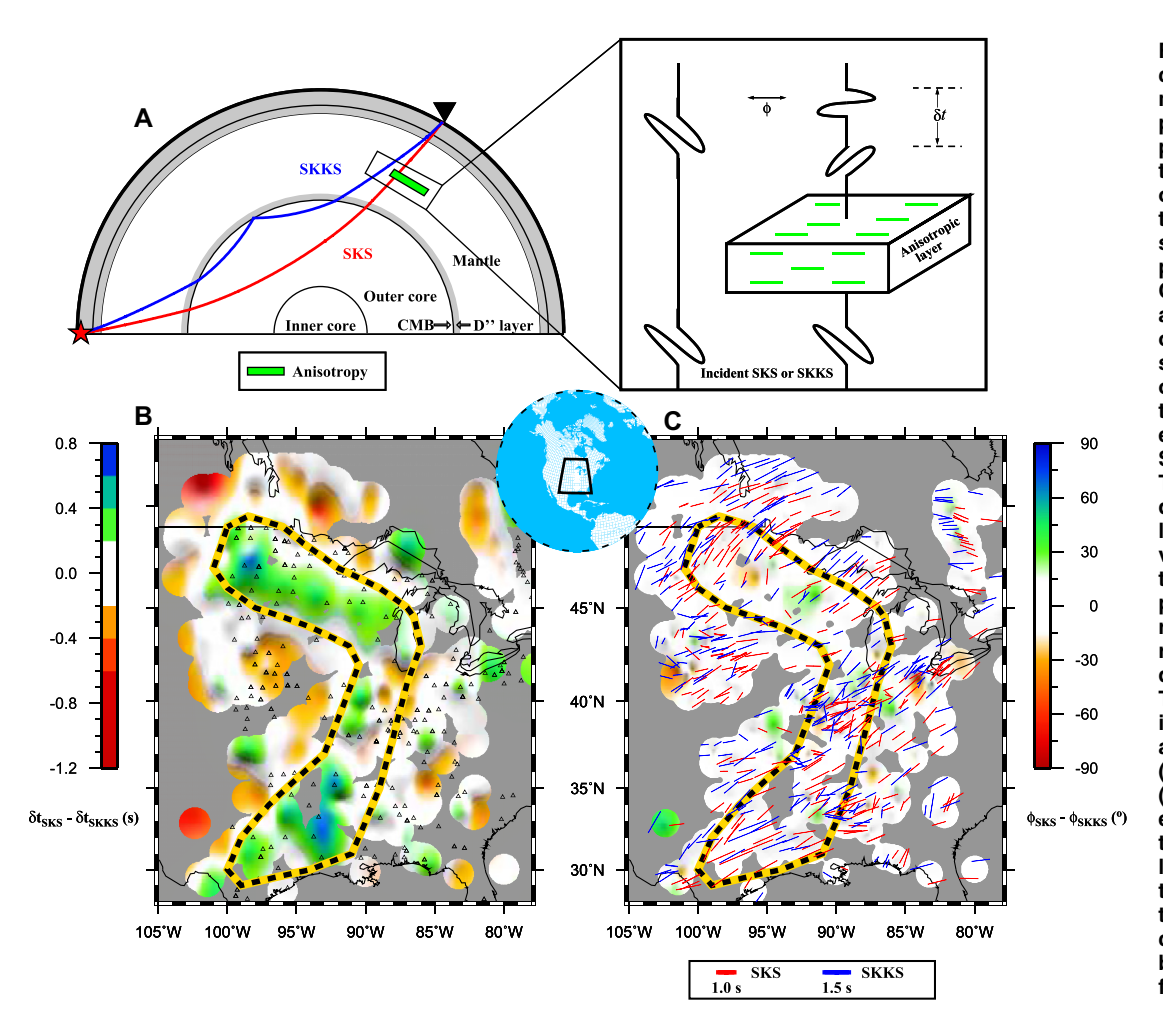


Figure 1. Illustration of discrepant SKS-SKKS splitting measurements. (A) Raypaths of SKS and SKKS phases. The SKS phase travels through a region of azimuthal anisotropy in the lower mantle (green segment), while the SKKS phase avoids this region. CMB—core-mantle boundary. A schematic diagram of shear-wave splitting is shown on the right. φ-fast orientation;  $\delta t$ —splitting time. (B) Observed differences between SKS and SKKS splitting delay times. The area outlined by the dashed black and yellow line is dominated by positive values of the SKS splitting time minus that of the SKKS phase. Black triangles represent station locations that recorded at least one welldefined SKS and SKKS pair. The enclosed area in the inset map shows the study area within North America. (C) SKS (red) and SKKS (blue) fast orientations. Orientation of bars represents the fast orientation, with the length being proportional to the magnitude of splitting time. Background color indicates the circular difference between the SKS and SKKS fast orientations.

segments: a flat-lying stagnant segment mostly in the uppermost lower mantle beneath the eastern United States, and a still-sinking segment beneath the western United States with a steeper dipping angle. These two segments may have separated at 70–50 Ma, and the gap between them is beneath the central United States (Sigloch et al., 2008).

#### METHODS AND RESULTS

We measured SKS and SKKS splitting patterns from 64 events recorded by 218 seismic stations that recorded at least one SKS and SKKS pair, resulting in 304 event-station pairs in total (Fig. S1 and Tables S1 and S2 in the Supplemental Material<sup>1</sup>). Differences between

'Supplemental Material. Tables S1 and S2 (the SKS and SKKS splitting pairs in the anomalous zone of Figure 1 and the pairs outside the zone) and Figures S1–S6 (earthquake distribution; examples of discrepant SKS-SKKS splitting measurements; discrepancy and number distributions in epicentral distance and back azimuth; estimation of anisotropy depth; and a schematic diagram showing the determined anisotropy depth based on the width of the discrepant region). Please visit https://doi.org/10.1130/GEOL.S.19400906 to access the supplemental material, and contact editing@geosociety.org with any questions.

the SKS and SKKS splitting parameters from the same event-station pair are shown in Figures 1B and 1C, and an example from station 733A can be found in Figure S2. While the fast orientations of the SKS and SKKS measurements are statistically consistent in the entire area (61.3°  $\pm$  22.8° for SKS and 61.9°  $\pm$  23.5° for SKKS) (Fig. 1C), the splitting time of SKKS (0.91  $\pm$  0.04 s) is dominantly smaller than that of SKS (1.13  $\pm$  0.05 s) for stations located in a large arc-shaped area (Fig. 1B, the area outlined by the dashed black and yellow line). In contrast, stations located outside this zone have indistinguishable splitting times.

To minimize the influences on the splitting times caused by waveform interference from non-SKS-non-SKKS phases (Lin et al., 2014), only events with an epicentral distance ranging from 100° to 130° and a focal depth >20 km were used (Deng et al., 2017; Grund and Ritter, 2019). As shown in Figure S3, the vast majority of the discrepant pairs are from events with an epicentral distance where the SKS or SKKS phase has an adequate time separation from the non-SKS-non-SKKS waves. In addition, we did not observe any sudden increase of the discrepancy from events with a back azimuth 30° or 45° apart from the fast orientation. The

observation would be expected if the increase in differential splitting times were caused by the interference of multiply reflected P waves (Fig. S3) (Tesoniero et al., 2020). Indeed, there is no systematic difference in both the azimuthal and the epicentral distance distributions between the non-discrepant and discrepant events (Fig. S4). Finally, interference by non-SKS—non-SKKS phases usually leads to SKKS times greater than SKS times (Lin et al., 2014; Tesoniero et al., 2020), while the opposite is observed in this study (Fig. 1). Thus, the observed greater SKS splitting times in the anomalous zone can hardly be attributed to interference by non-SKS—non-SKKS phases.

### DISCUSSION

Due to the nearly identical raypaths of the SKS and SKKS phases in the upper mantle, this discrepancy of splitting times between the SKS and SKKS phases from the same event-station pair in the anomalous zone (Fig. 1B) suggests the presence of an azimuthally anisotropic region in the lower mantle. Because the fast orientations from SKS and SKKS phases are virtually identical for the vast majority of the event-station pairs, the difference of the splitting times can be utilized to quantify the strength of a "residual"

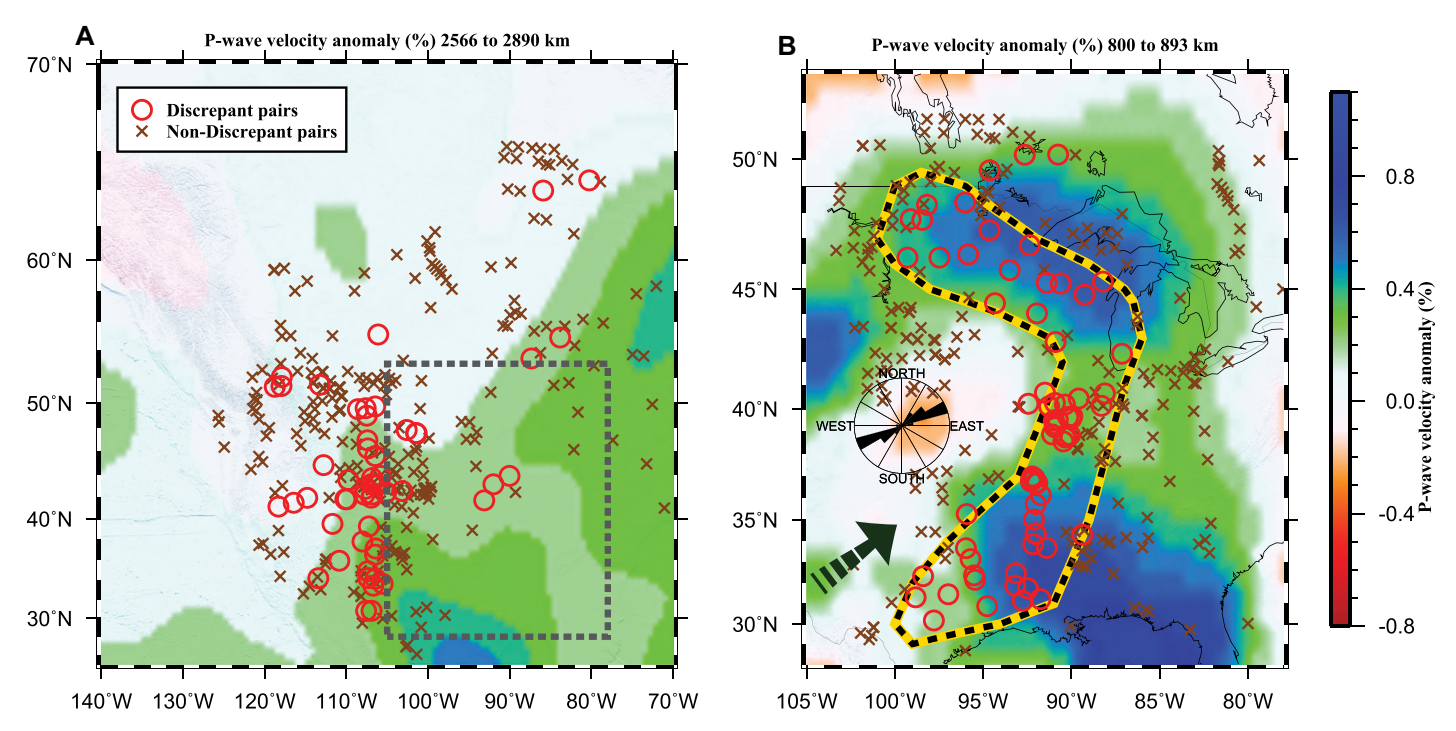


Figure 2. Spatial distribution of ray-piercing points for discrepant (circles) and non-discrepant (crosses) SKS-SKKS pairs at depths of 2700 km (A) and 850 km (B). Dashed quadrangle in A represents the region shown in B. Circles and crosses represent the middle of the ray-piercing points between the SKS and SKKS phases. Background color denotes the P-wave velocity anomaly for the depth layer of 2566–2890 km (A) and 800–893 km (B) in the GAP\_P4 model (Obayashi et al., 2013). Black and yellow dashed line shown in B stands for the area where the splitting time of the SKS phase is dominantly greater than that of the SKKS phase from the same event-station pair. The rose diagram in B exhibits the fast orientations of the discrepant SKS and SKKS shear-wave splitting measurements, and the arrow denotes the Mesozoic subduction direction of the Farallon plate from 64 Ma to 74 Ma (Bunge and Grand, 2000).

anisotropic layer. Under the assumption that the residual anisotropy is caused by a single layer with 4% anisotropy (Silver and Chan, 1991), the observed  $0.22\pm0.04$  s difference in the splitting time corresponds to an anisotropic layer with a thickness of  $\sim\!20\pm4.5$  km. If the anisotropy strength is in the range of 3% to 7% and the actual value is dependent on temperature, pressure, and shear strength (Savage, 1999), the estimated thickness of the layer is in the range of  $32.7\pm5.9$  to  $14\pm2.5$  km, respectively. In the following, we use the anisotropy strength of 4% where quantitative discussions of possible anisotropy formation mechanisms are required.

# Arguments Against a D" Origin of the Observed Differential Anisotropy

Previous seismic anisotropy studies have demonstrated that except for the D'' layer in the lowermost mantle (Fig. 1A) and areas directly beneath active subduction systems, the bulk of the lower mantle is azimuthally isotropic, indicating that the dominant deformation mechanism in the lower mantle is diffusion creep that cannot produce detectable seismic anisotropy (Girard et al., 2016). However, the observations presented in this study cannot be readily attributed to the D'' for the following reasons:

(1) The ray-piercing points of the discrepant SKS-SKKS measurements are concentrated in a narrow zone in the uppermost lower mantle and

are clearly separated from the piercing points of the non-discrepant measurements (Fig. 2B). In sharp contrast, the piercing points of these two types of measurements mingle with each other in the lowermost mantle (Fig. 2A).

(2) An uppermost lower-mantle origin of the discrepant splitting times is consistent with the estimated depth of the residual anisotropy. To quantify the depth of the residual anisotropy, we applied an anisotropy depth estimation procedure based on the spatial coherency of the splitting measurements (see the Supplemental Material for details) with candidate depths ranging from 500 to 2800 km. The resulting optimal depth that maximizes the spatial coherence of the discrepant  $\delta t$  is  $845 \pm 15$  km (Fig. S5), suggesting an origin in the uppermost lower mantle for the observed residual anisotropy.

(3) An uppermost lower-mantle rather than a D" origin of the observed discrepant splitting times is consistent with the width of the zone with discrepant splitting times (see the Supplemental Material and Fig. S6 for details).

# **Anisotropy Associated with the Farallon Slab in the Uppermost Lower Mantle**

The remarkable spatial correspondence between the area with discrepant splitting times between the SKS and SKKS phases and the western edge of a high-velocity zone in the uppermost lower mantle, which has been widely regarded as the stagnant Farallon slab in numerous seismic tomography studies (Sigloch et al., 2008; Obayashi et al., 2013; Lu et al., 2019), suggests a causative link between the slab and the discrepant splitting times. A possible explanation for the discrepant splitting times is an  $\sim$ 20-km-thick anisotropic layer in the Farallon lithosphere (Fig. 3). Along the western edge of the high-velocity zone, only the SKS but not the SKKS phase travels through the anisotropic layer, resulting in larger SKS splitting times (Fig. 3; Fig. S6). In the area to the west of the high-velocity zone ("the western area"), neither phase travels through the anisotropic layer, and to the east of this zone ("the eastern area"), both phases travel through this layer. This explains the observation that the SKS and SKKS splitting times are comparable in both the western and eastern areas (Fig. 3).

Geodynamic modeling studies (Bunge and Grand, 2000; L. Liu et al., 2008) indicate that the dominant direction of Farallon subduction was northeastward, which is consistent with the fast orientation of the observed azimuthal anisotropy (Fig. 2B). Thus, the most likely cause of the observed northeast-southwest-oriented differential azimuthal anisotropy is lattice-preferred orientation (LPO) of minerals or shape-preferred orientation (SPO) of rocks in or adjacent to the subducted slab. Bridgmanite and magnesiowüstite, the dominant minerals in the ambient

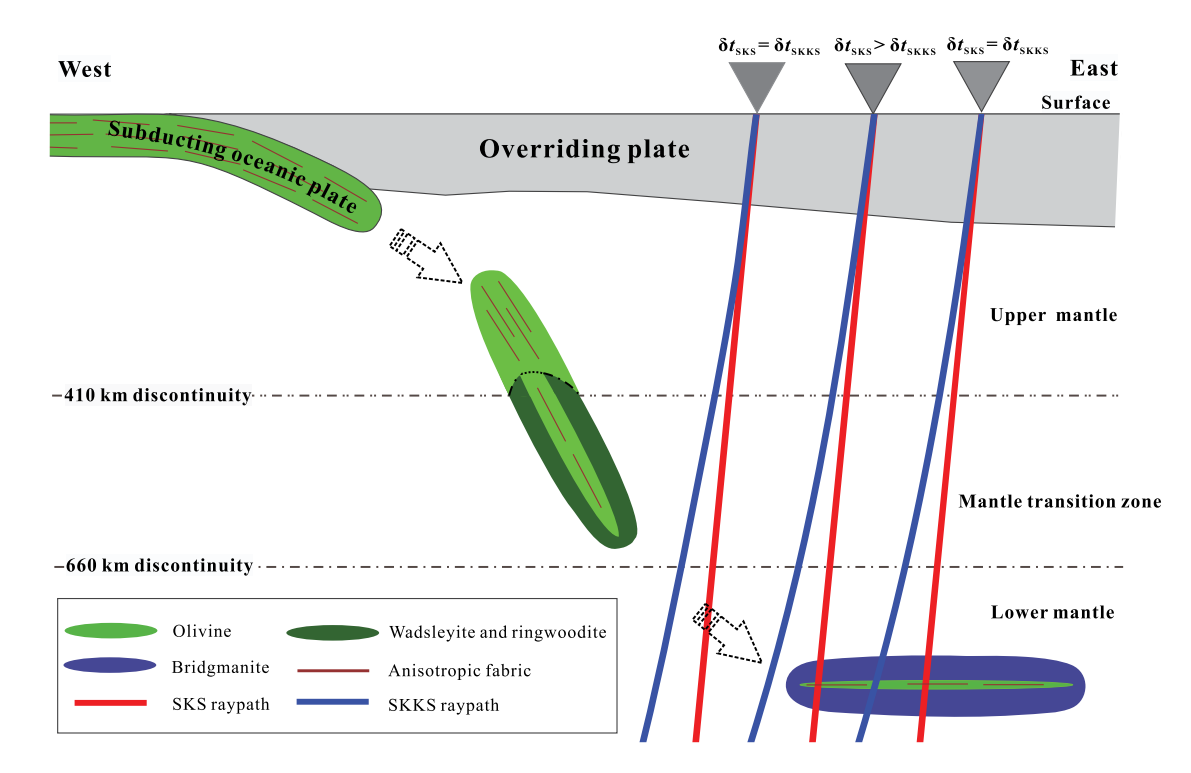


Figure 3. Schematic model illustrating the transformation of olivine during subduction and the cause of the discrepant SKS-SKKS splitting measurements. At the western station, neither the SKS nor SKKS phase travels through the slab and thus the splitting parameters (φ-fast orientation; δt-splitting time) are the same. For the middle station, the SKS phase travels through the slab and not the SKKS phase, resulting in greater SKS splitting time. For the eastern station, both SKS and SKKS phases travel through the slab, leading to identical SKS and SKKS splitting parameters.

uppermost lower mantle and the outermost layer of the slab, cannot lead to splitting of the subvertically propagating SKS or SKKS waves (Wookey et al., 2002; Yamazaki and Karato, 2002; Tsujino et al., 2016; Fu et al., 2019). A metastable ringwoodite layer inside the slab is largely isotropic (Mainprice, 2015), and LPO of wadsleyite under horizontal shear would produce a fast orientation perpendicular, rather than parallel, to the shear direction (Kawazoe et al., 2013). Therefore, the LPO of metastable ringwoodite or wadslevite under horizontal shear is inconsistent with the observed measurements. Similarly, grain-scale and rock-scale layering of basaltic materials in the MTZ and possibly the uppermost lower mantle is capable of producing radial but not azimuthal anisotropy (Faccenda et al., 2019). These leave us with the most likely candidate for the observed differential anisotropy, i.e., a layer of metastable olivine in the coldest core of the slab. It has been suggested that olivine LPO can develop by mantle flow parallel to the subduction direction (Yuan and Beghein, 2013), and thus anisotropy in this layer may represent the frozen-in anisotropy that was produced prior to subduction.

## GEODYNAMIC IMPLICATIONS AND CONCLUSIONS

This first evidence of the existence of a metastable olivine layer in the core of the subducted Farallon lithosphere in the uppermost lower mantle implies that the negative buoyancy associated with the low temperature (Obayashi et al., 2013; Lu et al., 2019) may be partially or entirely compensated by the low density of the metastable olivine layer. Some

previous laboratory and geodynamic modeling studies suggest that below a temperature of 1000 K, olivine may remain metastable under the uppermost lower-mantle pressure (Wang et al., 1997) and is characterized by lower density and lower seismic velocities than the rest of the slab. The scaling factor of P-wave velocity to temperature decreases with increasing depth, to about  $-0.23\% \pm 0.05\%/100 \text{ K}$ in the uppermost lower mantle (Cammarano et al., 2003). Thus, a P-wave velocity anomaly of +2% associated with the subducted Farallon slab (Schmandt and Lin, 2014) would result in a negative temperature anomaly of 710-1110 K. Using an ambient uppermost mantle temperature of ~1900 K (Boehler, 1996), the temperature at the core of the slab could be lower than the threshold value of 1000 K required for the existence of metastable olivine. Using these and other experimentally determined physical properties, we conclude that the magnitude of density deficiency associated with the metastable olivine layer is approximately comparable to the density increase for the rest of the slab due to the cold temperature (see the Supplemental Material for details), leading to a neutrally buoyant Farallon slab in the uppermost lower mantle.

### ACKNOWLEDGMENTS

This study was supported by the National Key R&D Program of China (grant 2017YFC1405502 to Y. Fang), the National Natural Science Foundation of China (grants 41890811 to J. Li, and 41976071 to F. Kong), and the U.S. National Science Foundation (grants 1919789 to S. Gao, 1830644 to K. Liu and S. Gao, and 2149587 to K. Liu). Critical reviews and comments from two anonymous reviewers greatly improved the manuscript.

#### REFERENCES CITED

Agrusta, R., van Hunen, J., and Goes, S., 2014, The effect of metastable pyroxene on the slab dynamics: Geophysical Research Letters, v. 41, p. 8800–8808, https://doi.org/10.1002 /2014GL062159.

Bina, C.R., and Kawakatsu, H., 2010, Buoyancy, bending, and seismic visibility in deep slab stagnation: Physics of the Earth and Planetary Interiors, v. 183, p. 330–340, https://doi.org/10.1016/j.pepi.2010.04.010.

Boehler, R., 1996, Melting temperature of the Earth's mantle and core: Earth's thermal structure: Annual Review of Earth and Planetary Sciences, v. 24, p. 15–40, https://doi.org/10.1146/annurev.earth.24.1.15.

Bunge, H.-P., and Grand, S.P., 2000, Mesozoic platemotion history below the northeast Pacific Ocean from seismic images of the subducted Farallon slab: Nature, v. 405, p. 337–340, https://doi.org/10.1038/35012586.

Cammarano, F., Goes, S., Vacher, P., and Giardini, D., 2003, Inferring upper-mantle temperatures from seismic velocities: Physics of the Earth and Planetary Interiors, v. 138, p. 197–222, https://doi.org/10.1016/S0031-9201(03)00156-0.

Deng, J., Long, M.D., Creasy, N., Wagner, L., Beck, S., Zandt, G., Tavera, H., and Minaya, E., 2017, Lowermost mantle anisotropy near the eastern edge of the Pacific LLSVP: Constraints from SKS-SKKS splitting intensity measurements: Geophysical Journal International, v. 210, p. 774–786, https://doi.org/10.1093/gji/ggx190.

Faccenda, M., Ferreira, A.M.G., Tisato, N., Lithgow-Bertelloni, C., Stixrude, L., and Pennacchioni, G., 2019, Extrinsic elastic anisotropy in a compositionally heterogeneous Earth's mantle: Journal of Geophysical Research: Solid Earth, v. 124, p. 1671–1687, https://doi.org/10.1029/2018JB016482.

Fu, S., Yang, J., Tsujino, N., Okuchi, T., Purevjav, N., and Lin, J.F., 2019, Single-crystal elasticity of (Al, Fe)-bearing bridgmanite and seismic shear wave radial anisotropy at the topmost lower mantle: Earth and Planetary Science Letters, v. 518,

- p. 116–126, https://doi.org/10.1016/j.epsl.2019 .04.023.
- Girard, J., Amulele, G., Farla, R., Mohiuddin, A., and Karato, S., 2016, Shear deformation of bridgmanite and magnesiowüstite aggregates at lower mantle conditions: Science, v. 351, p. 144–147, https://doi.org/10.1126/science.aad3113.
- Grund, M., and Ritter, J.R.R., 2019, Widespread seismic anisotropy in Earth's lowermost mantle beneath the Atlantic and Siberia: Geology, v. 47, p. 123–126, https://doi.org/10.1130/G45514.1.
- Iidaka, T., and Suetsugu, D., 1992, Seismological evidence for metastable olivine inside a subducting slab: Nature, v. 356, p. 593–595, https://doi.org/10.1038/356593a0.
- Ito, E., and Katsura, T., 1989, A temperature profile of the mantle transition zone: Geophysical Research Letters, v. 16, p. 425–428, https://doi.org/10.1029 /GL016i005p00425.
- Jiang, G., Zhao, D., and Zhang, G., 2008, Seismic evidence for a metastable olivine wedge in the subducting Pacific slab under Japan Sea: Earth and Planetary Science Letters, v. 270, p. 300–307, https://doi.org/10.1016/j.epsl.2008.03.037.
- Kaneshima, S., Okamoto, T., and Takenaka, H., 2007, Evidence for a metastable olivine wedge inside the subducted Mariana slab: Earth and Planetary Science Letters, v. 258, p. 219–227, https://doi .org/10.1016/j.epsl.2007.03.035.
- Kawazoe, T., Ohuchi, T., Nishihara, Y., Nishiyama, N., Fujino, K., and Irifune, T., 2013, Seismic anisotropy in the mantle transition zone induced by shear deformation of wadsleyite: Physics of the Earth and Planetary Interiors, v. 216, p. 91–98, https://doi.org/10.1016/j.pepi.2012.12.005.
- Kirby, S.H., Stein, S., Okal, E.A., and Rubie, D.C., 1996, Metastable mantle phase transformations and deep earthquakes in subducting oceanic lithosphere: Reviews of Geophysics, v. 34, p. 261–306, https://doi.org/10.1029/96RG01050.
- Lin, Y.P., Zhao, L., and Hung, S.H., 2014, Full-wave effects on shear wave splitting: Geophysical Research Letters, v. 41, p. 799–804, https://doi.org/10.1002/2013GL058742.

- Liu, K.H., Gao, S.S., Gao, Y., and Wu, J., 2008, Shear wave splitting and mantle flow associated with the deflected Pacific slab beneath northeast Asia: Journal of Geophysical Research, v. 113, B01305, https://doi.org/10.1029/2007JB005178.
- Liu, L., Spasojević, S., and Gurnis, M., 2008, Reconstructing Farallon plate subduction beneath North America back to the Late Cretaceous: Science, v. 322, p. 934–938, https://doi.org/10.1126/science.1162921.
- Long, M.D., and Lynner, C., 2015, Seismic anisotropy in the lowermost mantle near the Perm Anomaly: Geophysical Research Letters, v. 42, p. 7073– 7080, https://doi.org/10.1002/2015GL065506.
- Lu, C., Grand, S.P., Lai, H., and Garnero, E.J., 2019, TX2019slab: A new *P* and *S* tomography model incorporating subducting slabs: Journal of Geophysical Research: Solid Earth, v. 124, p. 11,549–11,567, https://doi.org/10.1029/2019JB017448.
- Mainprice, D., 2015, Seismic anisotropy of the deep Earth from a mineral and rock physics perspective, *in* Price, D., and Stixrude, L., eds., Treatise on Geophysics (second edition), Volume 2: Mineral Physics: Amsterdam, Elsevier, p. 487–538, https://doi.org/10.1016/B978-0-444-53802-4 00044-0
- Obayashi, M., Yoshimitsu, J., Nolet, G., Fukao, Y., Shiobara, H., Sugioka, H., Miyamachi, H., and Gao, Y., 2013, Finite frequency whole mantle *P* wave tomography: Improvement of subducted slab images: Geophysical Research Letters, v. 40, p. 5652–5657, https://doi.org/10.1002/2013GL057401.
- Ringwood, A.E., 1975, Composition and Petrology of the Earth's Mantle (first edition): New York, McGraw-Hill, 672 p.
- Savage, M., 1999, Seismic anisotropy and mantle deformation: What have we learned from shear wave splitting?: Reviews of Geophysics, v. 37, p. 65–106, https://doi.org/10.1029/98RG02075.
- Schmandt, B., and Lin, F.C., 2014, P and S wave tomography of the mantle beneath the United States: Geophysical Research Letters,

- v. 41, p. 6342–6349, https://doi.org/10.1002/2014GL061231.
- Sigloch, K., McQuarrie, N., and Nolet, G., 2008, Twostage subduction history under North America inferred from multiple-frequency tomography: Nature Geoscience, v. 1, p. 458–462, https://doi .org/10.1038/ngeo231.
- Silver, P.G., and Chan, W.W., 1991, Shear wave splitting and subcontinental mantle deformation: Journal of Geophysical Research, v. 96, p. 16,429–16,454, https://doi.org/10.1029/91JB00899.
- Tesoniero, A., Leng, K., Long, M.D., and Nissen-Meyer, T., 2020, Full wave sensitivity of *SK(K)S* phases to arbitrary anisotropy in the upper and lower mantle: Geophysical Journal International, v. 222, p. 412–435, https://doi.org/10.1093/gji/ggaa171.
- Tsujino, N., Nishihara, Y., Yamazaki, D., Seto, Y., Higo, Y., and Takahashi, E., 2016, Mantle dynamics inferred from the crystallographic preferred orientation of bridgmanite: Nature, v. 539, p. 81–84, https://doi.org/10.1038/nature19777.
- Wang, Y., Martinez, I., Guyot, F., and Liebermann, R.C., 1997, The breakdown of olivine to perovskite and magnesiowüstite: Science, v. 275, p. 510–513, https://doi.org/10.1126/science.275 .5299.510.
- Wookey, J., Kendall, J.-M., and Barruol, G., 2002, Mid-mantle deformation inferred from seismic anisotropy: Nature, v. 415, p. 777–780, https:// doi.org/10.1038/415777a.
- Yamazaki, D., and Karato, S.-i., 2002, Fabric development in (Mg,Fe)O during large strain, shear deformation: Implications for seismic anisotropy in Earth's lower mantle: Physics of the Earth and Planetary Interiors, v. 131, p. 251–267, https://doi.org/10.1016/S0031-9201(02)00037-7.
- Yuan, K., and Beghein, C., 2013, Seismic anisotropy changes across upper mantle phase transitions: Earth and Planetary Science Letters, v. 374, p. 132–144, https://doi.org/10.1016/j.epsl.2013 05 031

Printed in USA